2021 43rd Annual International Conference of the
IEEE Engineering in Medicine & Biology Society (EMBC)
Oct 31 - Nov 4, 2021. Virtual Conference

Empirical Mode Decomposition Based Hyperspectral Data Analysis for Brain Tumor Classification

Nauman Baig[1], Himar Fabelo[2], Samuel Ortega[2], Gustavo M. Callico[2], Javad Alirezaie[1], Karthikeyan Umapathy[1]

Abstract— **The capability of Hyperspectral Imaging (HSI) in rapidly acquiring abundant reflectance data in a non-invasive manner, makes it an ideal tool for obtaining diagnostic information about tissue pathology. Identifying wavelengths that provide the most discriminatory clues for specific pathologies will greatly assist in understanding their underlying biochemical characteristics. In this paper, we propose an efficient and computationally inexpensive method for determining the most relevant spectral bands for brain tumor classification. Empirical mode decomposition was used in combination with extrema analysis to extract the relevant bands based on the morphological characteristics of the spectra. The results of our experiments indicate that the proposed method outperforms the benchmark in reducing computational complexity while performing comparably with a 7-times reduction in the feature-set for classification on the test data.**

Index Terms— **Hyperspectral imaging, feature selection, empirical mode decomposition, pattern classification**

I. INTRODUCTION

It is estimated that 1 out of 157 people is expected to develop some variation of brain carcinoma within Canada [1]. Surgery, chemotherapy, and radiotherapy are some of the common treatments with surgery being the primary option for tumor resection. The conventional surgical method involves taking a biopsy of the location of interest and removing as much of visible tumor as possible through resection. However, this does not guarantee complete removal of the tumor tissue and often leaves behind cancer residue that grows undetected [2]. Alternatively, over-resection of the brain tissue can cause irreversible damage to functional brain tissue. Novel tumor delineation techniques such as intra-operative MRIs have been more effective in accurate delineation but have limitations such as poor spatial resolution, and extended surgery times [3].

As a noninvasive and nonionizing imaging modality, Hyperspectral Imaging (HSI) offers great potential in pathology diagnostics due to its ability to quantify optical characteristics of different biomaterials [4]. Certain biomaterials, such as tumors, exhibit unique reflectance characteristics at specific wavelengths. Identifying these wavelengths can lead towards efficient classification of biomaterials and their exact pixel-based location within hyperspectral (HS) images, allowing for precise surgical operations.

[1]Department of Electrical, Computer and Biomedical Engineering, Ryerson University, Toronto, ON, M5B2K3, Canada

[2]Research Institute for Applied Microelectronics, University of Las Palmas de Gran Canaria, Las Palmas de Gran Canaria, Spain

Recent advances have proven the efficacy of HSI-based classification within medical applications such as disease diagnosis [4]. In [5], an unsupervised classification system using K-means clustering was used on HS data to determine the exact location of tumors within breast cancer images. Wang et al. utilized a grayscale segmentation algorithm on HSI images to segment liver tumor with a high degree of accuracy [6]. Additionally, there are a few related works that have proposed the use of decomposition-based methods within HSI analysis for medical diagnosis. Spectral unmixing has been used in [7] to develop spatial maps for classifying liver cancer data, and in [8] to estimate the concentration of hemoglobin and melanin within tissue for cancer diagnosis. However, these methods required prior knowledge of the spectral characteristics of biochemicals or tissues.

With regards to utilizing HS analysis for brain cancer diagnosis, Fabelo et al. developed various brain cancer detection algorithms to be used on HS images within surgical operations [9], [10]. However, these methods required high computational cost as they had to incorporate all 128 bands within their analysis. In [11], Martinez et al. proposed the use of optimization algorithms to identify relevant wavelengths that achieve the best multi-class pixel classification accuracy while employing the least amount of spectral bands. Using the same HSI brain database, they evaluated different optimization algorithms and explored the effect of different classification parameters, such as sampling intervals and number of features, on classification performance. This research work will serve as a benchmark for the work presented in this paper.

In this work, we introduce a novel computationally inexpensive decomposition-based method for automatically identifying spectral bands that result in a higher discrimination between different tissue types. By identifying the most relevant spectral bands for tumor diagnosis, the size of HS data can be reduced even further, making both acquisition and analysis far less computationally expensive. This is done by first using EMD (Empirical Mode Decomposition) to quantify oscillatory characteristics of spectra into Intrinsic Mode Functions (IMFs). Then, the most relevant spectral bands for discriminating between different tissue types are extracted by analyzing the extrema of the IMFs. Finally, the reflectance values of the filtered spectra at the determined relevant bands are then selected as features for pixel classification.

978-1-7281-1178-0/21/$31.00 ©2021 IEEE

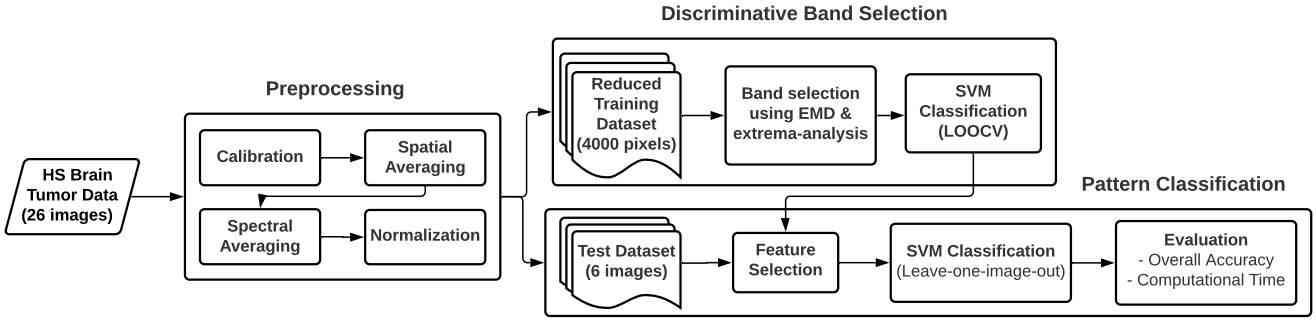

Fig. 1. Framework of the proposed methodology.

II. METHODOLOGY

The framework of the proposed method is outlined in Fig. 1. The procedure is comprised of three main stages; data preprocessing, band selection, and pattern classification. The data, selection of spectra, and the preprocessing steps, were all similar to that of the benchmark to allow for a fair comparison.

A. Database

Data used for our analysis was obtained from the HSI Human Brain Database that was developed by researchers at the University of Las Palmas de Gran Canaria, within the context of the European project HELICoiD [12]. The data consisted of HS images of brain tissues from patients that had to undergo craniotomy for intra-axial brain tumor resection or another brain surgery type at the University Hospital of Gran Canaria Doctor Negrin (Spain). The extracted reflectance data from the images contained 826 spectral bands ranging between 400 and 1,000 nm, including ground truth information for four classes: tumor, normal, hypervascularized (or blood vessel) tissue, and background pixels. More details about the dataset can be found in [12].

Twenty-six HS images obtained from sixteen adult patients were employed to extract labelled spectral reflectance profiles. Spectra of a total of 269,967 labelled pixels were extracted, consisting of: 101,706 normal (38%), 11,054 tumor (4%), 39,084 hypervascularized (14%), and 118,132(44%) background pixels. Two different subsets were created similar to the procedure in the benchmark's method [11] in order to be able to compare the results. The first subset consisted of extracting 4,000 pixels from all 26 images with equal distribution among all four class types. This reduced dataset was used within the band selection procedure. The second subset consisted of six different HS images from four patients affected by grade IV Glioblastoma brain tumor which are then used as test data for pattern classification following a leave-one-image-out cross-validation methodology.

B. Preprocessing

A series of preprocessing steps were performed over the HS data to remove unwanted noise and obtain uniform reflectance-based spectral signatures for feature extraction. Firstly, images are calibrated using Equation (1) where I_{raw} is the raw image, I_{white} is the white reference image, and I_{dark} is the dark reference image acquired using the acquisition system [11].

$$CalibratedImage = \frac{I_{raw} - I_{dark}}{I_{white} - I_{dark}} \tag{1}$$

A combination of spectral and spatial filtering techniques was applied for noise removal. High-frequency noise introduced by the HS camera is removed by applying a linear-regression based smoothing filter to each pixel [13]. The HS images are then spatially filtered by taking the average reflectance value of neighboring pixels in order to remove random noise.

The spectrum of each pixel is then averaged within the spectral domain and downsampled to 128 bands, which was determined as reported in [11] to be the optimal number of bands as it provides a suitable compromise between execution time and overall accuracy for pixel classification. Finally, the data is normalized over each HS image by clipping any outliers exceeding three standard deviations from the mean of the spectra, centering the spectra around the mean, and scaling of reflectance between 0 and 1. Apart from the spatial filtering step, all other preprocessing steps are practically the same as in [11], where the specific procedures and rationale are explained in detail.

C. Discriminative Band Selection

The first stage of feature selection (from discriminative bands) consists of applying EMD to each spectra. EMD is a nonlinear adaptive signal analysis method for decomposing signals into components based on the oscillatory characteristics of the signals [14]. Compared to other decomposition methods, such as wavelet decomposition, EMD was chosen for this work as it provides a method of extracting oscillatory characteristics using far less computational power. The basis of EMD is a sifting procedure that splits a signal into IMFs. These IMFs have two ideal characteristics; the number of local extrema between each IMF differ by one at most, and the mean value of the two envelopes extracted from the extrema is zero. The procedure of generating IMFs is described as follows:

1) Identifying Local Extrema: First, the spectra of a pixel is fed as an input. Sifting begins with the identification

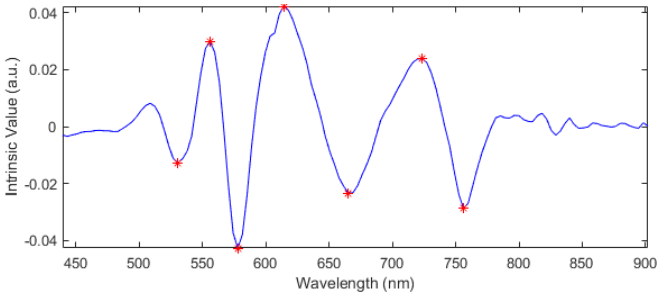

Fig. 2. Selected Bands (red), identified by the proposed extrema-based feature selection algorithm, on a sample decomposed IMF.

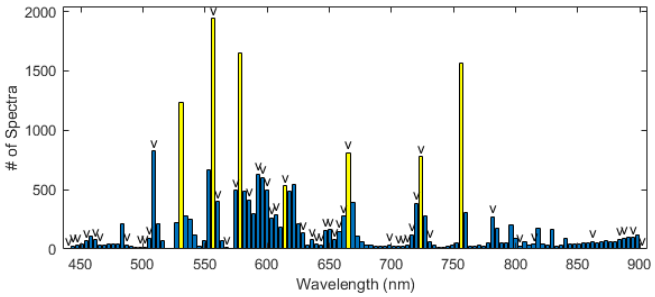

Fig. 3. Histogram of the extrema count of all IMFs in the reduced training dataset. The optimal bands selected by the proposed method are highlighted in yellow and the 48 bands selected by the implemented benchmark method are marked with a 'v'.

of local extrema, such as maxima and minima, of the signal.

2) Calculating Residual: The extrema are interpolated such that a connection of all the maxima forms the upper envelop, whereas a connection of all the minima forms the lower envelop. The mean of the two envelopes is computed to obtain a residual signal.
3) Obtaining IMF: The residual is then subtracted from the initial spectra to get the resulting detail. If the sifting criteria is met, sifting stops and the remaining detail is treated as the first IMF.
4) Sift on Residuals: The remaining residual is then used as the signal and sifting using steps 2 and 3 are performed to acquire the next IMF. This is iterated until the maximum number of IMFs has reached.

The sifting criteria is determined by the relative tolerance which is calculated using euclidean distance. A predetermined threshold is set to stop sifting once the computed mean falls under the threshold and the criteria is met. If the sifting criteria is not met after step 3, steps 2 and 3 are iterated again on the residual until the criteria is met and the procedure can move on to generate following IMFs. The full procedure is performed on the spectra of each pixel, until the entire image has been decomposed. Since the sifting criteria allows for including different frequency components within an IMF, only the first IMF is considered and other IMFs were not computed.

The second stage of feature selection involves identifying the most relevant bands based on the discriminatory morphology observed within the IMF. The critical, or turning, points observed within the IMF are representative of the morphological changes observed within the spectra. Thus, an extrema-based featured selection algorithm is developed to identify the locations of such critical points.

First, the average IMF of all spectra is computed for each spectral band. Then, the extrema of the average IMF are identified based on a specific prominence threshold. The prominence describes the significance of an extremum based on its height and location relative to neighboring peaks. More specifically, the prominence of a peak, or local maximum, is calculated by taking the difference of the IMF value of a peak and the IMF value of the highest neighboring valley in the signal. Prominence of the valleys, or local minima, are determined by inverting the signal and performing the same calculation.

As the prominence threshold is increased, the number of extrema identified decreases. Depending on how many extrema are identified, the locations of these extrema are selected as relevant bands of interest. The plot in Fig. 2 shows the distribution of the selected bands whereas Fig. 3 illustrates the coincidence of the selected bands with the extrema count within each band for all 4,000 curves. The optimal bands seem to coincide with the prominent extrema of a significant number of curves, proving that they are highly representative. Additionally, four of the seven optimal bands were found to be mutual with the 48 bands suggested by the implemented benchmark method.

Finally, the reflectance values of the filtered spectra at the determined relevant bands are then selected as features for pixel classification.

D. Pattern Classification

For fair comparison with the benchmark in [11], a linear kernel Support Vector Machine (SVM) algorithm is employed to quantify the discriminatory ability of the selected features. The classifier is implemented using the LIBSVM package developed by Chang et al [15], along with leave-one-out cross-validation on the reduced dataset and leave-one-image-out cross-validation on the test dataset. In leave-one-image-out cross-validation, labelled pixels of one image from the test dataset are classified while the remaining five images are used for training the classifier.

The results of the classification are evaluated quantitatively by calculating the overall accuracy and determining its computational time. Overall accuracy (OA) was calculated using equation (2) where y is the predicted label and T is the ground truth for sample k.

$$OA = \frac{1}{n}\sum_{k=0}^{n} x_k \begin{cases} x_k = 1, & \text{if } y_k = T_k \\ x_k = 0, & \text{if } y_k \neq T_k \end{cases} \quad (2)$$

The resulting six overall accuracies obtained using the leave-one-image-out cross-validation method are averaged to obtain a final overall accuracy.

III. RESULTS AND DISCUSSION

The experiments are performed within MATLAB version R2019b running on a 64-bit Windows 10 workstation consisting of Intel Core i7 CPU and 8GB of RAM. For fair comparison, both the proposed method and the benchmark method are computed on the same platform.

TABLE I

PERFORMANCE OF VARIOUS PROMINENCE VALUES ON THE REDUCED DATASET

Prominence (a.u.)	0.0025	0.0045	0.0125	0.0425	0.0485
# of bands generated	21	10	7	4	2
Overall Accuracy (%)	87.8	87.2	85.4	84.8	53.9

TABLE II

COMPARISON OF RESULTS

		EMD-based Analysis	Benchmark
# of bands		7	48
Reduced Data	OA	85.4%	**90.5%**
	Time	**39.5s**	>60min
Test Data	OA	**73.36%**	73.1%
	Time	**147.3s**	335.5s

Table I displays the classification performance on reduced training dataset for various prominence threshold used to select the number of bands. As the prominence threshold is increased, the amount of bands selected decreased. This is attributed to the fact that less extrema are picked up as the threshold is increased. Adjusting the threshold value allows for limiting the number of features selected. Although the accuracy results for the different prominence values was similar, a value of 0.0125 is chosen within our analysis as it provided a good balance between accuracy and number of bands generated. The chosen values generated a total of 7 extreme values within the average IMF, resulting in 7 optimal bands for classification.

Using the 7 bands, a final overall accuracy of 73.36% is obtained with a total computation time of 186.8 (39.5 + 147.3) seconds. Table II summarizes these results along with the results of the benchmark method which was implemented and evaluated using our framework. Compared to the benchmark, the proposed method provides a much faster way of extracting the most relevant bands. Additionally, it achieves comparable classification accuracy using just 7 bands (in comparison with 48 bands) at much less cost. Classifying just the 3 bands that were non-mutual with the 48 benchmark bands resulted in an overall accuracy of 62% on the test data, demonstrating that this method could also identify relevant bands that were undetected by the benchmark.

IV. CONCLUSION

In this paper, we proposed a novel decomposition-based method of automatically identifying the most relevant spectral bands for classifying HS images of in-vivo human brain tumors. Firstly, EMD is applied within the spectral domain of the data to extract IMFs that quantify oscillatory characteristics of the reflectance data. Then, the most relevant bands are identified based on the location of extrema present within the average IMF. Classification results of the proposed method shows that EMD enhances the feature selection process for identifying relevant spectral bands for tissue classification. Additionally, it provided comparable classification in terms of overall accuracy using the test dataset at much reduced computational cost using only 7 bands. Future work consists of testing the performance of this method on other HS cancer data, fine tuning the parameter selection, and determining band correlation with biochemical composition of pathologies.

ACKNOWLEDGMENT

The authors would like to thank Natural Sciences and Engineering Research Council of Canada (NSERC), Ryerson University, and University of Las Palmas de Gran Canaria (ULPGC) for supporting this research.

V. REFERENCES

[1] S. Canada, C. C. Society, *et al.*, "Release notice-canadian cancer statistics 2019.," *Health promotion and chronic disease prevention in Canada: research, policy and practice*, vol. 39, no. 8-9, p. 255, 2019.

[2] N. Sanai and M. S. Berger, "Operative techniques for gliomas and the value of extent of resection," *Neurotherapeutics*, vol. 6, no. 3, pp. 478–486, 2009.

[3] M. Reinges, H.-H. Nguyen, T. Krings, B.-O. Hütter, V. Rohde, and J. Gilsbach, "Course of brain shift during microsurgical resection of supratentorial cerebral lesions: Limits of conventional neuronavigation," *Acta neurochirurgica*, vol. 146, no. 4, pp. 369–377, 2004.

[4] G. Lu and B. Fei, "Medical hyperspectral imaging: A review," *Journal of biomedical optics*, vol. 19, no. 1, p. 010 901, 2014.

[5] Y. Khouj, J. Dawson, J. Coad, and L. Vona-Davis, "Hyperspectral imaging and k-means classification for histologic evaluation of ductal carcinoma in situ," *Frontiers in oncology*, vol. 8, p. 17, 2018.

[6] J. Wang, M. Hu, M. Zhou, L. Sun, and Q. Li, "Segmentation of pathological features of rat bile duct carcinoma from hyperspectral images," in *2018 11th International Congress on Image and Signal Processing, BioMedical Engineering and Informatics (CISP-BMEI)*, IEEE, 2018, pp. 1–5.

[7] I. Kopriva, G. Aralica, M. P. Hadžija, M. Hadžija, L.-I. Dion-Bertrand, and X. Chen, "Hyperspectral imaging for intraoperative diagnosis of colon cancer metastasis in a liver," in *Medical Imaging 2019: Digital Pathology*, International Society for Optics and Photonics, vol. 10956, 2019, 109560S.

[8] G. Lu, X. Qin, D. Wang, Z. G. Chen, and B. Fei, "Estimation of tissue optical parameters with hyperspectral imaging and spectral unmixing," in *Medical Imaging 2015: Biomedical Applications in Molecular, Structural, and Functional Imaging*, International Society for Optics and Photonics, vol. 9417, 2015, 94170Q.

[9] H. Fabelo, S. Ortega, D. Ravi, B. R. Kiran, C. Sosa, D. Bulters, G. M. Callicó, H. Bulstrode, A. Szolna, J. F. Piñeiro, *et al.*, "Spatio-spectral classification of hyperspectral images for brain cancer detection during surgical operations," *PLoS One*, vol. 13, no. 3, e0193721, 2018.

[10] H. Fabelo, M. Halicek, S. Ortega, M. Shahedi, A. Szolna, J. F. Piñeiro, C. Sosa, A. J. O'Shanahan, S. Bisshopp, C. Espino, *et al.*, "Deep learning-based framework for in vivo identification of glioblastoma tumor using hyperspectral images of human brain," *Sensors*, vol. 19, no. 4, p. 920, 2019.

[11] B. Martinez, R. Leon, H. Fabelo, S. Ortega, J. F. Piñeiro, A. Szolna, M. Hernandez, C. Espino, A. J O'Shanahan, D. Carrera, *et al.*, "Most relevant spectral bands identification for brain cancer detection using hyperspectral imaging," *Sensors*, vol. 19, no. 24, p. 5481, 2019.

[12] H. Fabelo, S. Ortega, A. Szolna, D. Bulters, J. F. Piñeiro, S. Kabwama, A. JO'Shanahan, H. Bulstrode, S. Bisshopp, B. R. Kiran, *et al.*, "In-vivo hyperspectral human brain image database for brain cancer detection," *IEEE Access*, vol. 7, pp. 39 098–39 116, 2019.

[13] S. Devika and S. Chaitanya, "Signal estimation of hyperspectral data using hysime algorithm," in *2016 International conference on research advances in integrated navigation systems (RAINS)*, IEEE, 2016, pp. 1–3.

[14] A. Zeiler, R. Faltermeier, I. R. Keck, A. M. Tomé, C. G. Puntonet, and E. W. Lang, "Empirical mode decomposition-an introduction," in *The 2010 International Joint Conference on Neural Networks (IJCNN)*, IEEE, 2010, pp. 1–8.

[15] C. Chang and C. Lin, "Libsvm: A library for support vector machines," *ACM transactions on intelligent systems and technology (TIST)*, vol. 2, no. 3, pp. 1–27, 2011.